Structural Engineering and Mechanics, *Vol. 65, No. 6 (2018) 741-750*
DOI: https://doi.org/10.12989/sem.2018.65.6.741

Dynamic responses of shield tunnel structures with and without secondary lining upon impact by a derailed train

Qixiang Yan*[1], Binjia Li[1a], Zhixin Deng[1b] and Bin Li[2c]

[1]*Key Laboratory of Transportation Tunnel Engineering, Ministry of Education, Southwest Jiaotong University, Chengdu, Sichuan, 610031, China*
[2]*The Third Railway Survey and Design Institute Group Corporation, Tianjin, 300000, China*

(Received July 28, 2016, Revised January 12, 2018, Accepted January 16, 2018)

Abstract. The aim of this study was to investigate the mechanical responses of a high-speed railway shield tunnel subjected to impact by a derailed train, with emphasis on the protective effect of the secondary lining. To do so, the extended finite element method was used to develop two numerical models of a shield tunnel including joints and joint bolts, one with a cast-in-situ concrete secondary lining and one without such a lining. The dynamic responses of these models upon impact were analyzed, with particular focus on the distribution and propagation of cracks in the lining structures and the mechanical responses of the joint bolts. The numerical results showed that placing a secondary lining significantly constricted the development of cracking in the segmental lining upon the impact load caused by a derailed train, reduced the internal forces on the joint bolts, and enhanced the safety of the segmental lining structure. The outcomes of this study can provide a numerical reference for optimizing the design of shield tunnels under accidental impact loading conditions.

Keywords: train impact load; assembled-segmental lining; fracture mechanics; crack characteristics of lining concrete; dynamic responses

1. Introduction

The rapid development of high-speed railway construction in China in recent years has led to the planning and construction of many tunnel projects. Because shield tunnels are constructed by assembling prefabricated lining segments, their overall stability and resistance to impact load are not as good as those of composite linings constructed by the mining method (Zhao *et al.* 2017, Yan *et al.* 2017, 2018). In particular, the impact load caused by a derailed high-speed train may result in fracturing of joint bolts, damage to joint plates, cracking of individual segments and collapse of the lining structure.

Many of the shield tunnels that have been constructed recently in China have incorporated a cast-in-situ concrete secondary lining over the segmental lining structure. Tunnels with such structures include, the Shiziyang Tunnel on the Guangzhou–Shenzhen-Hong Kong passenger transport line, the Qiantang River Tunnel on the Hangzhou-Changsha passenger transport line, the Huangpu River Tunnel on the Shanghai-Nantong Railway and the Qiongzhou Strait Cross-Sea Tunnel. An important role of the secondary lining is to improve the integrity of shield tunnel. To date, there is a lack of complete studies on the dynamic responses of a double-lined shield tunnel subjected to the impact load caused by a derailed high-speed train, and this limits the development of double-lined shield tunnels to some extent.

Takamatsu *et al.* (1992) investigated the mechanical behavior of a double-lined shield tunnel in the longitudinal direction by performing a structural model test. They proposed a design method in which joints were placed at particular positions in the secondary lining to reduce the internal forces in the lining. Koizumi and He (2000) used shaking-table model tests and finite element method (FEM) simulations to analyze the dynamic responses of a double-lined shield tunnel in the longitudinal direction in irregular ground. In the context of constructing the Shiziyang Tunnel, which is the first underwater, high-speed railway shield tunnel in China, Feng *et al.* (2013) conducted laboratory reduced-scale model tests and field full-scale tests to investigate the mechanical behavior of double-lined shield tunnel subjected to hydrostatic water pressure. Yan *et al.* (2015) proposed an improved numerical model for double-lined shield tunnels, and they verified the model by experimental results from reduced-scale model tests.

Studies on train impacts have been focused mainly on investigating the crashworthiness of trains. Milho *et al.* (2003) proposed a multibody numerical model for trains that contained anti-impact components, and they verified the model by comparing the results of simulations with experimental data. Based on the United States Standard, Gao and Tian (2007) selected acceleration and absorbed energy as criteria for the anti-impact evaluation of trains, and they improved the anti-impact design technology for trains. Simulation tests for energy-absorbing components were conducted by Gupta and Venkatesh (2006) on energy-

*Corresponding author, Professor
E-mail: 1428271635@qq.com
[a]Ph.D. Student
[b]M.S. Student
[c]Engineer

ISSN: 1225-4568 (Print), 1598-6217 (Online)

absorbing tubes, and by Hong *et al.* (2008) on aluminum honeycomb material. Xie and Zhou (2014) applied these energy-absorbing components to trains and conducted effective simulation calculations. Baykasoğlu *et al.* (2011) verified the accuracy of FEM simulation of the train carriage behavior in a crash with an experimental examination, and then they analyzed and improved the crashworthiness design for trains using FEM.

With regard to structures impacted by trains, Yan *et al.* (2016) studied the dynamic responses of a double-lined shield tunnel upon impact caused by derailed trains at different speeds. The traditional FEM has some shortcomings in dealing with nonlinear cracking of concrete, e.g., the large amount of calculation and the limited ability to simulate the dynamic cracking process. To overcome these shortcomings, Belytschko and Black (1999) proposed the extended finite element method (XFEM) to solve discontinuous problems within the framework of traditional FEM. Moës *et al.* (1999, 2002) simulated the nonlinear cracking of a concrete member by embedding the cohesive crack model into XFEM. Zia *et al.* (2005) used XFEM to simulate the propagation of dynamic cracks. The results indicated that XFEM is capable of capturing mixed-mode fracturing caused by impact load. Areias and Belytschko (2005) also applied XFEM to simulate the dynamic propagation process of 3D cracks in brittle and quasi-brittle materials. Subsequently, XFEM has been developed rapidly and is used extensively to simulate dynamic crack propagation and nonlinear cracking in concrete.

To the authors' knowledge, no study has been reported that attempted to investigate the cracking damage of double-lined shield tunnel and dynamic responses of joint bolts when impacted by a derailed train. In this study, we attempted to mitigate this gap and provide a numerical reference for the design of the secondary lining. To do so, it was necessary to compare the crack features of the segmental lining and the mechanical responses of the joint bolts with and without applying a secondary lining.

2. Dynamic analysis models of a tunnel by the extended finite element method (XFEM)

2.1 Extended finite element theory

In the nonlinear FE software ABAQUS, the initiation and propagation process of cracks in tunnel linings upon impact load can be simulated by XFEM, which increases the computational efficiency by introducing the discontinuous displacement model into the traditional FE analysis. The discontinuous displacement field is no longer dependent on re-meshing in XFEM, and the mesh-dependence problem is avoided. XFEM approximation is based on the partition of unity method. According to the partition of unity method, the displacement can be approximately stated as

$$u^h(x) = \sum_{i=1}^{N} N_i(x)\big(u_i + a_i\Phi_i(x)\big) \tag{1}$$

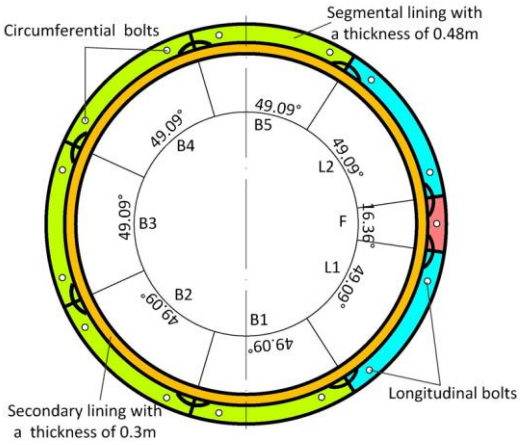

Fig. 1 Relationship between the segmental lining and the cast-in-situ concrete secondary lining

where $N_i(x)$ is the finite element shape function of i^{th} node; u_i is the displacement of the i^{th} node; a_i is the additional degree of freedom of the i^{th} node; $\Phi_i(x)$ is the enrichment function for the i^{th} node; and N is the set of all nodes. For any point x within the domain

$$\sum_i N_i(x) = 1 \tag{2}$$

If the enrichment functions are set as the progressive functions reflecting the surface and tip of the crack, the displacement can be stated as

$$u(x) = \sum_{i\in N} N_i(x)u_i + \sum_{j\in N^{dts}} N_j(x)H(x)a_j + \sum_{k\in N^{asy}} N_k(x)\sum_{\alpha=1}^{4}\Phi_\alpha(x)b_k^a \tag{3}$$

where $N_i(x)$, $N_j(x)$, and $N_k(x)$ are the finite element shape functions of the i^{th}, j^{th}, and k^{th} nodes, respectively; N^{dts} and N^{asy} are the node sets of elements thoroughly penetrated by cracks and elements with crack tips, respectively; a_j is the improved dof of the j^{th} node related to the Heaviside function; b_k^a is the improved degree of freedom of the k^{th} node related to the elastic progressive function of crack tip; $H(x)$ is the improved function; and $\Phi_\alpha(x)$ is the progressive displacement field function that reflects the singularity of the stress of the crack tip.

2.2 Dynamic analysis models of tunnel

This study was focused on a specific tunnel in China with the aim of assessing the effects of the secondary lining on the dynamic responses of a shield tunnel impacted by a train. Two numerical models of the shield tunnel upon impact load were established, one of which contained a cast-in-situ concrete secondary lining while the other did not.

Since XFEM can describe the discontinuous displacement field without re-meshing, it is capable of

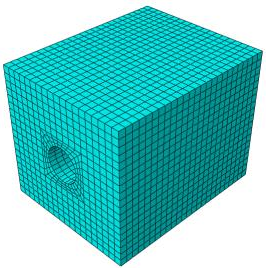

(a) Surrounding ground elements

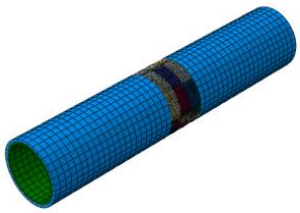

(b) Segmental lining elements

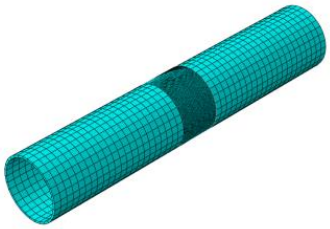

(c) Secondary lining elements

Fig. 2 Numerical models of a shield tunnel

simulating the fracturing process of concrete quite well. Therefore, the XFEM was used to simulate the cracking of shield tunnel linings. In the case with a secondary lining, as shown in Fig. 1, the thickness of the secondary lining was 0.3 m, and the secondary lining was installed on the inner surface of the segmental lining. In the case in which there was no secondary lining, the tunnel consisted of a single segmental lining that had outer diameter, inner diameter, thickness, and width along the longitudinal direction dimensions of 10.3, 9.34, 0.48, and 2.0 m, respectively. The segmental ring consisted of five standard segments B1-B5 (49.09°), two counter key segments L1-L2 (49.09°) and one key segment F (16.36°) (see Fig. 1). The tunnel was excavated through the sediments of quaternary upper Pleistocene Q3 and Holocene series Q4, which consisted mainly of sandy soil, weathered argillaceous silt, and other minor components.

Fig. 2 shows the numerical models of the shield tunnel that were subjected to the impact of the train. For the model without a secondary lining, the numerical model consisted of the surrounding ground elements and the segmental lining elements. For the model with a secondary lining, the model consisted of the surrounding ground elements, the segmental lining elements, and the secondary lining elements. The length, width, and height dimensions of both models were 90, 60, and 60 m, respectively. The boundaries were simulated by continuously distributed equivalent spring-damper systems. The equivalent spring-damper system is a kind of artificial boundary system that is usually used to simulate the effect of an infinite soil mass on the

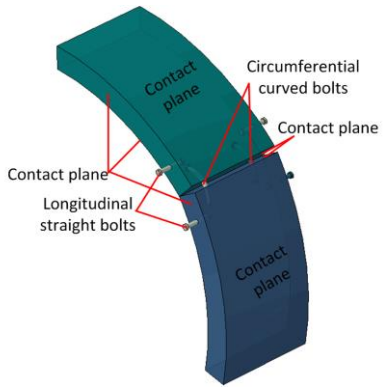

Fig. 3 3D contact relationships between the segments and surrounding ground

finite calculation model, which consists of springs and dampers in the normal and tangential directions, and it has proved to be capable of meeting the precision requirement of engineering.

To simulate the actual structure as precisely as possible while avoiding the significant decrease of computational efficiency due to a large number of joint interfaces in the segmental lining, the segmental ring subjected to the train impact (the "target ring"), together with two adjacent rings, were simulated as assembled segments. The rest of the joints in the segmental lining were treated approximately by weakening the concrete elements with the equivalent flexural rigidity method.

The 3D contact relationships used in the models are shown in Fig. 3. In order to shorten the processing time of large amounts of contact in the models, we used a contact search algorithm that divided the contact planes into principal and subordinate planes. The contact model used between the three segmented lining rings and the anteroposterior linings is a binding constraint. The binding constraint contact model binds the nodes of the subordinate plane to the principal plane, and there is no relative displacement between the two contact planes.

The plane-plane contact method was used to simulate the interaction between the target ring and the two adjacent rings, the interaction between the segments in the same segmental lining ring, and the interaction between the segmental lining and secondary lining, using the hard contact model in the normal direction and the Coulomb friction contact (friction coefficient 0.6) model in the tangential direction. Once the compressive stress becomes zero or negative in the hard contact model, the two contact planes are separated, and the contact constraint between the corresponding nodes is removed.

The joint bolts were simulated with solid elements, and the contact between bolts and segmental linings was simulated by embedding both ends of each bolt into the corresponding segment elements. In so doing, the tensile, compressive, and shear mechanical properties of the bolts were simulated along with the deformation state of the bolts under various stress conditions. The interaction between the segmental lining and the surrounding ground was simulated by plane-plane contact model, using the penalty stiffness model in the normal direction and the Coulomb friction

contact model (friction coefficient 0.8) in the tangential direction. The following formulas can be used to describe the penalty stiffness model

$$\begin{cases} p = 0 & (\Delta l < 0) \\ p > 0 & (\Delta l = 0) \\ p = f(k, \Delta l) & (\Delta l > 0) \end{cases} \quad (4)$$

where p is the contact force; Δl is the embedded volume; k is the penalty stiffness; and f is the penalty function.

The Mohr-Coulomb elastoplastic constitutive relationship was used for the surrounding ground, and the concrete elastoplastic constitutive relationship was used for the segmental lining and secondary lining. The stress-strain relationship of concrete was selected from GB 50010-2010 (2010). The joint bolts were assumed to be linearly elastic. Cracking of the segmental lining and the secondary lining was simulated by XFEM. The fracture energies, i.e., G_{If}, G_{IIf}, and G_{IIIf}, were assumed to be 80 N/m (Cendón *et al.* 2006). The material parameters of surrounding ground, linings, and joint bolts are listed in Table 1.

The impact load of the train was decomposed into component forces in the X-, Y-, and Z-directions, which were applied in the form of average surface force on the inner surfaces of lining structures on the actual impact area. Fig. 4 shows the segmental rings, the relevant bolts, the direction the train was traveling, and the center of the impact region. For the model with a secondary lining, the center of the impact region was the projection of the marked area onto the inner surface of the secondary lining. In Fig. 4, rings ①, ②, and ③ are segmental rings connected by joint bolts. Ring ② is the impacted target ring. J1, J2, and J3 are longitudinal joints. M1 and M2 are the curved bolts in ring ② at joint J2. M3 and M4 are the curved bolts at joint J3. L1 and L2 are the longitudinal straight bolts before and after the key segment (relative to the direction the train was traveling). L3 and L4 are the longitudinal straight bolts before and after the impacted segment in ring ②.

2.3 Train Impact load

Currently, numerical simulation studies at present usually obtain the impact load of the train using a 3D model of a train impacting a rigid wall. Yan *et al.* (2016) established a numerical model as shown in Fig. 5. Their numerical model of the train consisted of one locomotive and eight carriages. The length, width, height, and coupler centerline space of the locomotive were 25.4, 3.4, 3.7, and 25.7 m, respectively, while the length, width, height, and coupler centerline space of the carriages were 24.5, 3.4, 3.7, and 25 m, respectively (Yan *et al.* 2018). The outer shape of the train made of aluminum alloy was simulated by thin-shell elements, and the foam-core material and glass fiber-reinforced plastics were used to obtain the equivalent stiffness and mass distribution of a real train. In addition, the couplers between the carriages were simulated by nonlinear springs, and the stiffness and damping of springs were 2000 kN/m and 40 kNs/m, respectively. The material properties used in the numerical model are provided in Table 2.

Table 1 Material parameters used in the models

Material	E^*(MPa)	v^*	Density (kg/m^3)	Cohesion (MPa)	φ^*
Sandy soil	25	0.35	2000	0	28°
Silt	35	0.35	2500	8	38°
Segment	34500	0.20	2500	-	-
Secondary lining	31000	0.20	2500	-	-
Bolt	206000	0.17	7850	-	-

*E: Elastic modulus; v: Poisson's ratio; φ: Friction angle

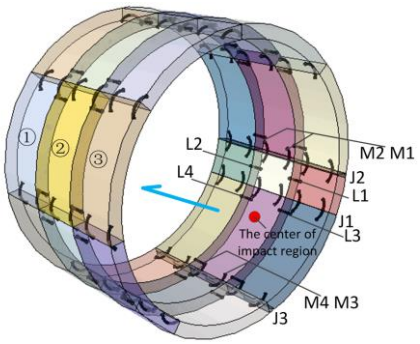

Fig. 4 Numbering of segmental lining rings and joint bolts

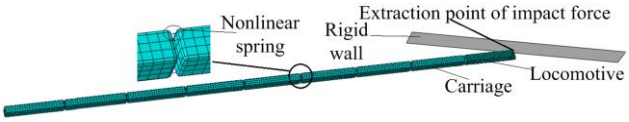

Fig. 5 Three-dimensional numerical model of a train impacting a rigid wall

Table 2 Material properties of the train model (Yan *et al.* 2016)

Material	E^*(MPa)	v^*	Density (kg/m^3)	Yield strength (MPa)
Aluminum alloy	70000	0.30	2700	225
Foam core	105	0.25	27	-
Glass fiber-reinforced plastics	8400	0.40	1600	150

*E: Elastic modulus; v: Poisson's ratio

The results of the numerical study indicated that the impact load caused by a derailed train was related largely to the train's configuration, the impact velocity, and the impact angle. Yan *et al.* (2016) presented a time-history curve of impact force in the case of the train's velocity being 200 km/h, an oblique impact angle of 12.5°, and eight carriages (see Fig. 6). It can be seen that the effective impact time is approximately 32 ms, where 1.2 ms is considered to be a boundary, i.e., the first 1.2 ms, including the peak, are defined as the peak stage of the impact load, and the rest of the impact load is defined as the shock stage. The impact force reaches its peak at the moment a train strikes a rigid wall due to the impact effect of the front several carriages, and it decreases sharply after reaching the peak value with the dissipation of kinetic energy of the front several carriages, which forms the peak stage of impact force. Then, the inertial force of subsequent carriages passes

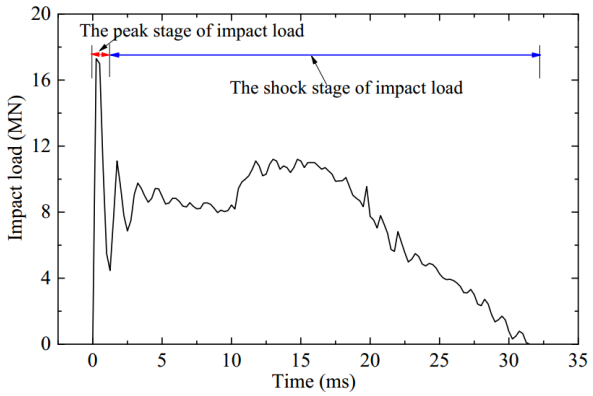

Fig. 6 Time-history curve of oblique impact load for a train traveling at a velocity of 200 km/h

through the coupler to the impact region and dissipates gradually, thus the shock stage of impact force is formed. According to the following numerical simulation, the dynamic responses of joint bolts are very different at the different stages of train impact load, which should be analyzed separately, so the impact load is divided into two stages for the convenience of the following research.

3. Comparison of crack features of the segmental lining

Fig. 7 presents the main cracked region of the segmental lining for the structures with and without the secondary lining. In the figure, the parameters of STATUSXFEM represent the degree of element cracking; when the value of STATUSXFEM is 0.0, there are no cracks, while the element is damaged completely when the value is 1.0. Fig. 7(a) (without the secondary lining) shows that the cracking in lining segments occurred mainly at the centre of the impact region and at joints J2 and J3, and the cracks at joint J3 were interrupted at ring ②. Since the centre of the impact region is the most heavily affected area, this crack is referred to as the main crack. Fig. 7(b) shows that no main crack was observed at the centre of the impact region, and no elements were damaged completely by cracking at the joints in the case with the secondary lining. The crack distributions of the segmental lining indicate that the circumferential joints can prevent the main crack from propagating into the neighbouring ring, and the secondary lining can distribute the impact load uniformly over the segmental lining.

The crack openings at joints J2 and J3 for the structures with and without the secondary lining were compared in order to analyze the effect of the secondary lining on restricting crack openings. Along the direction the train was traveling, monitoring points B1-B3 were located on the crack on the surface of joint J2, and B4-B6 were located on the crack outside the segment near the surface of the joint. Since the crack distributions on ring ① and ring ③ are similar at joint J3, only the crack openings of ring ③ were analyzed. Monitoring points C1 and C3 were located at the positions of the curved bolt, and C2 was located at the

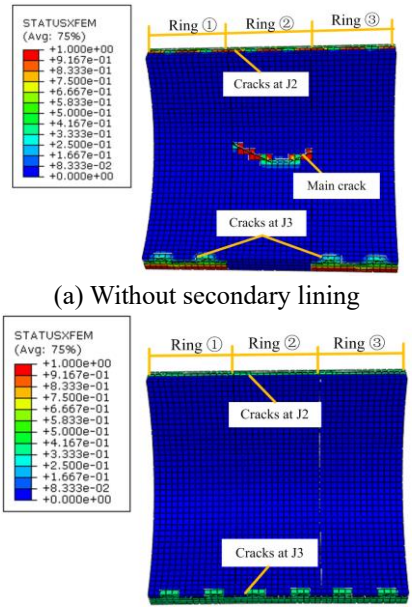

Fig. 7 Comparison of crack distributions of the segmental lining

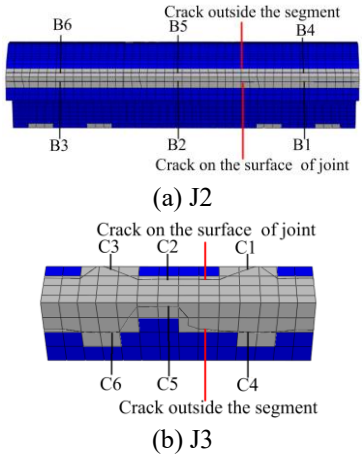

Fig. 8 Crack monitoring points at the joint

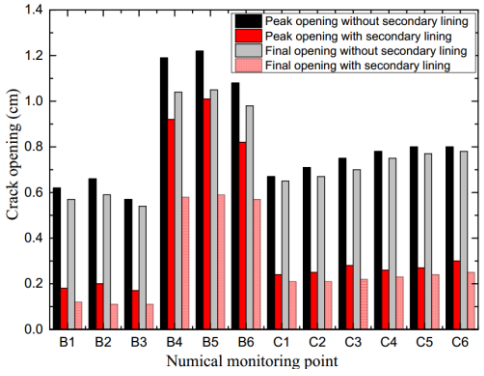

Fig. 9 Peak and final crack openings at the monitoring points at joints J2 and J3

midpoint of the segment. Monitoring points C4-C6 were located at the corresponding positions outside the segment. These configurations are shown in Fig. 8.

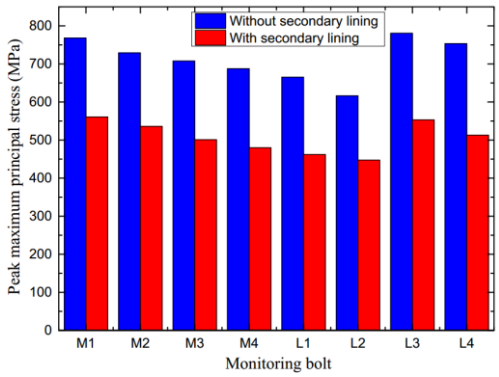

Fig. 10 Comparison of peak maximum principal stresses in the bolts

Fig. 9 shows the peak and final openings of the cracks at the monitoring points. In both cases, i.e., with and without the secondary lining, the differences between the crack openings on the surfaces of the joints and outside the segment at J3 were smaller than those that at J2. When the secondary lining was used, the peak and final crack openings at B1-B3 were reduced by about 70% and 80%, respectively. The peak and final openings at B4-B6 were reduced by about 20% and 40%, respectively. At J3, the peak and final openings at C1-C6 were reduced by about 65% and 68%, respectively. The results indicated that the peak and final openings of cracks in joints were reduced significantly by the secondary lining, and the reductions of the final crack openings were larger than those of the peak crack openings.

4. Comparison of dynamic responses of joint bolts

According to the calculation of dynamic responses of all the joint bolts for the structures with and without the secondary lining, eight bolts with the largest dynamic responses (curved bolts M1-M4 and straight bolts L1-L4) were selected for analysis. The monitoring point of each bolt was set at the center of the middle cross-section. Fig. 10 shows the peak maximum principal stresses in selected bolts for the structures with and without the secondary lining. Whether or not a secondary lining is present, the peak σ1 (maximum principal stress) in the rear bolt (relative to the direction in which the train was traveling) was greater than that in the front bolt at the same horizontal position due to the oblique impact of the train. For example, the peak σ1 in bolt M1 was greater than that in M2, and the peak σ1 in bolt L3 was greater than that in L4. Thus, as Fig. 10 shows, the least favourable curved bolt is M1, and the least favourable straight bolt is L3.

There was no reason to analyze the σ1 time-history curves for all of the bolts in the structure, so only the least favourable bolts (M1 and L3) were analyzed. Fig. 11 shows the time-history curves of $\sigma 1$ in M1 and L3 for the structures with and without the secondary lining. Since there were large differences between the amplitudes of σ1 in the bolt at different stages of impact load, for the sake of clarity, Fig. 11 presents the curves at the peak and shock

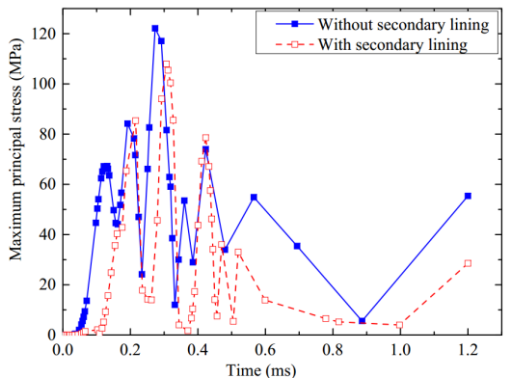

(a) M1 at the peak stage of impact load

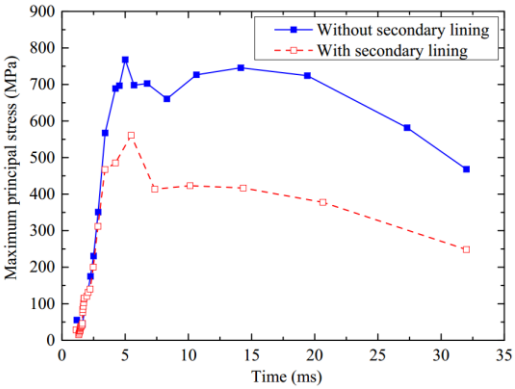

(b) M1 at the shock stage of impact load

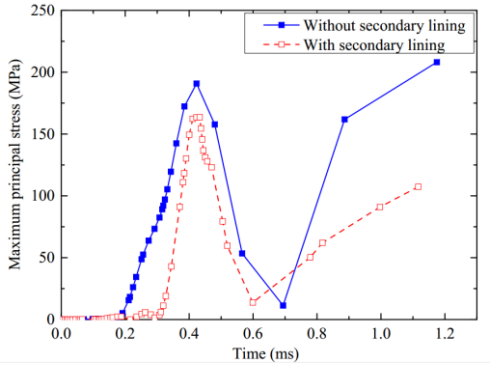

(c) L3 at the peak stage of impact load

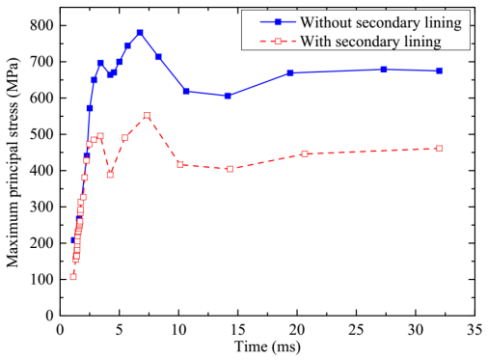

(d) L3 at the shock stage of impact load

Fig. 11 Comparison of time-histories of maximum principal stress of the least favorable bolts

stages separately. It should be noted that the method used to process the velocity and acceleration time-history curves was the same as that of σ1.

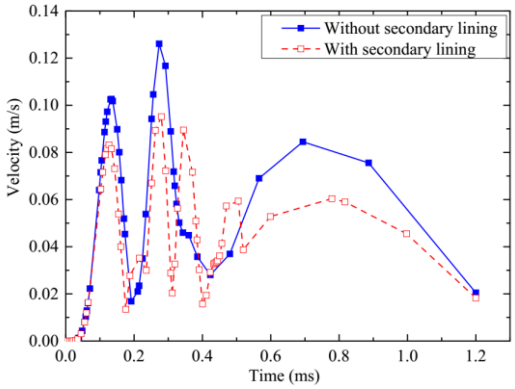

(a) M1 at the peak stage of impact load

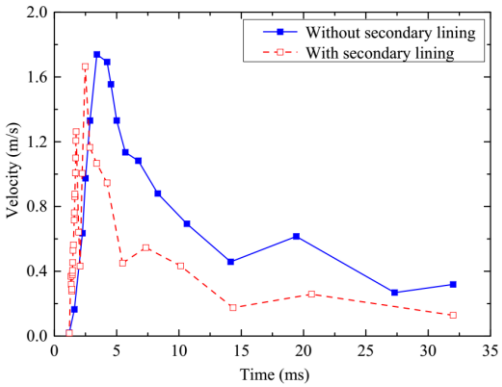

(b) M1 at the shock stage of impact load

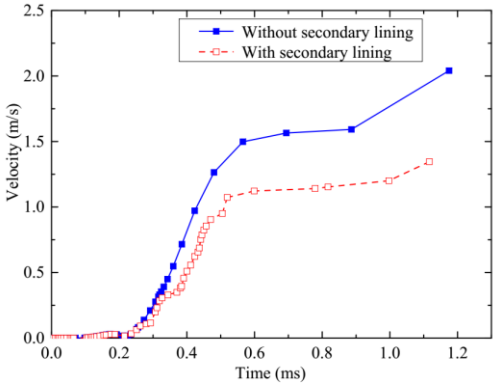

(c) L3 at the peak stage of impact load

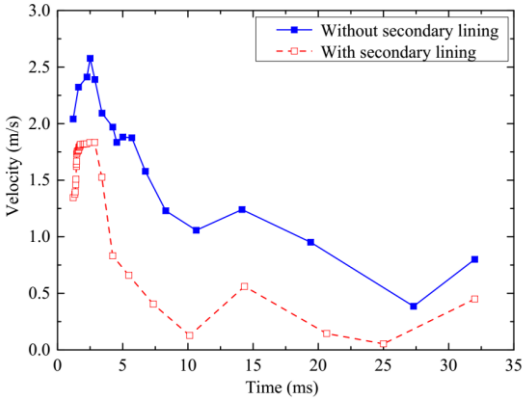

(d) L3 at the shock stage of impact load

Fig. 12 Comparison of time-histories of velocity of the least favorable bolts

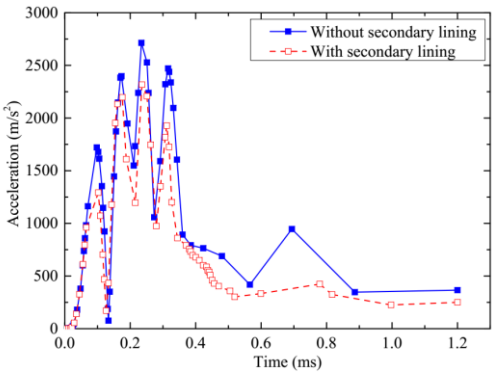

(a) M1 at the peak stage of impact load

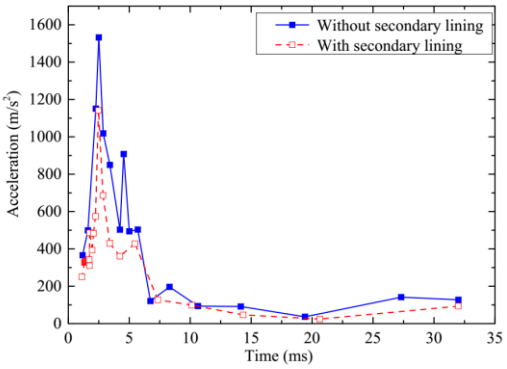

(b) M1 at the shock stage of impact load

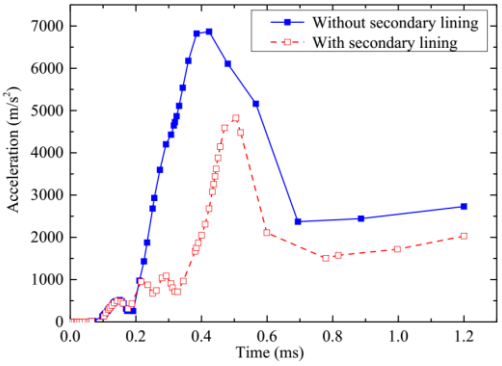

(c) L3 at the peak stage of impact load

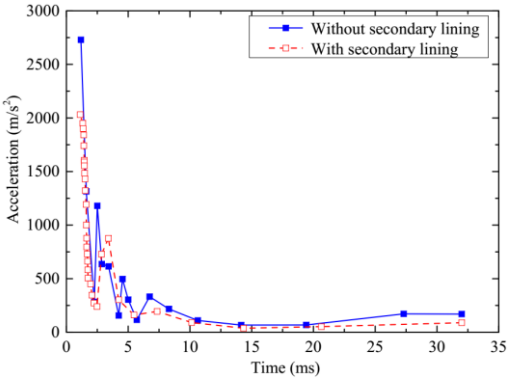

(d) L3 at the shock stage of impact load

Fig. 13 Comparison of time-histories of acceleration of the least favorable bolts

As shown in Fig. 11, the variations of $\sigma 1$ time-history curves of the least favorable bolts for both structures are similar. The $\sigma 1$ peaks occurred at the shock stage of impact load rather than the peak stage. During the entire impact

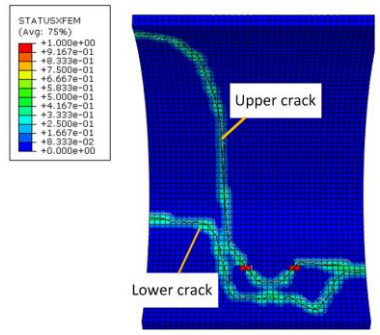

(a) Inner surface

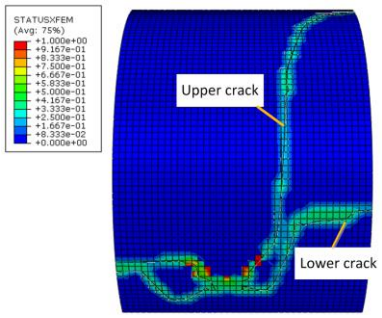

(b) Outer surface

Fig. 14 Distribution of cracks in the secondary lining

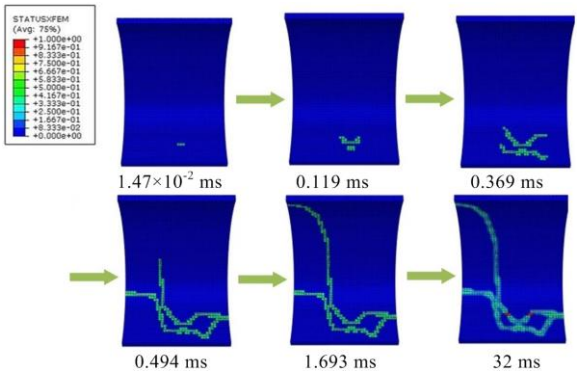

(a) Inner surface

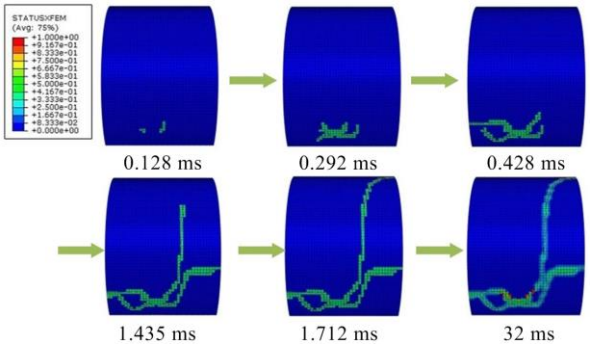

(b) Outer surface

Fig. 15 Crack propagation on the inner and outer surfaces of the secondary lining

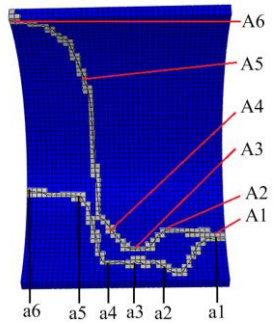

Fig. 16 Crack monitoring points on the inner surface of the secondary lining

process, the σ1 values in bolts were reduced by the presence of the secondary lining, and the reductions were more obvious at the shock stage of the impact load. The peak values of $\sigma 1$ were reduced by approximately 27% in M1 and 29% in L3 by using the secondary lining. The peak value of σ1 in M1 was close to that in L3.

Fig. 12 shows the velocity time-history curves of the least favorable bolts M1 and L3 for the structures with and without a secondary lining. It is observed from the figure that the variations of the velocity time-history curves of the least favorable bolts for both structures are similar. The peak velocities occurred at the shock stage of the impact load. During the entire impact process, the velocities of bolts were reduced by the presence of the secondary lining, and the reductions were more obvious at the shock stage of the impact load. The peak velocities were reduced by about 27% for M1 and 29% for L3 by using the secondary lining. In addition, the velocity of L3 was greater than that of M1.

Fig. 13 shows the acceleration time-history curves of bolts M1 and L3 for the structures with and without a secondary lining. Contrary to the σ1 and velocity curves, the peak accelerations occurred at the peak stage rather than the shock stage of the impact load. The effects of the impact load on the accelerations of the bolts can be seen mainly in the first 10 ms of impact. The acceleration of L3 generally was greater than that of M1. During the entire impact process, the acceleration of the bolt was reduced when the secondary lining was used, and the peak acceleration was reduced by about 25% for M1 and 30% for L3.

5. Crack features of the secondary lining

When a train strikes a shield tunnel that has a secondary lining, the secondary lining is directly affected by the impact load. Analysis of the segmental lining cracks is discussed above, so this section only discusses the cracks of the secondary lining. Fig. 14 shows the crack distribution of the secondary lining subjected to train impact load. Two cracks (upper and lower) are seen in the secondary lining. The shapes of the inner surface and outer surface cracks imply that they are transfixion cracks. Because there are no joints in the secondary lining, these two cracks differ from those in the outer segmental lining. Whereas the latter are discontinuous at the circumferential joints, cracks in the secondary lining tend to propagate continuously.

Fig. 15 shows the dynamic propagation process of cracks on the inner and outer surfaces of the secondary lining. Initially, the force of the train's impact initiated a microcrack on the inner surface at the center of impact region within 1.47×10^{-2} ms. Then, another microcrack

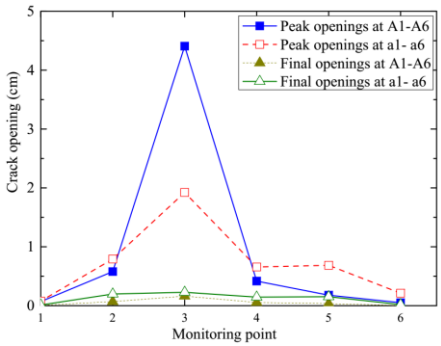

Fig. 17 Peak and final crack openings at the monitoring points

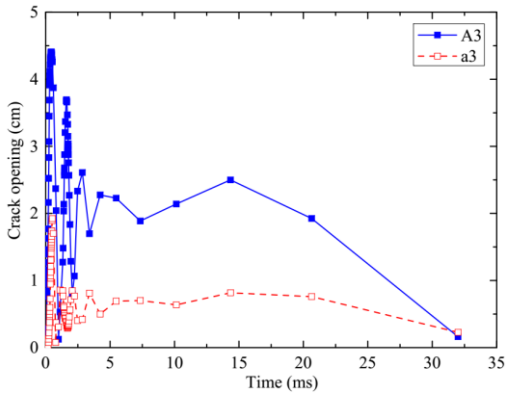

Fig. 18 Time-history curves of crack opening at monitoring points A3 and a3

appeared above the first microcrack, and these two microcracks propagated upwards and towards both sides. At 1.693 ms, the upper and lower cracks stopped propagating. Finally, these two cracks tended to connect in the middle. The appearance time of microcracks on the outer surface was later than that on the inner surface. The microcracks on the outer surface of the secondary lining appeared at 0.128 ms, and then propagated towards the center to form two continuous cracks. Finally, these two continuous cracks propagated to become the upper and lower cracks.

Fig. 16 shows the positions of the points at which the cracks were monitored on the inner surface of the secondary lining. Monitoring points A1-A6 and a1-a6 were set on the upper and lower cracks along the direction the train was traveling, respectively. The progress of crack propagation in the secondary lining described above indicated that the cracks on the outer and inner surfaces are transfixion cracks that follow the same crack propagation behavior, differing only in the magnitude of opening. Therefore, only the crack openings at the monitoring points on the inner surface of the secondary lining are discussed in the following.

Fig. 17 shows the peak and final crack openings at the monitoring points. The maximum peak opening occurred at A3, while the maximum final opening occurred at a3. A3 and a3 were the two monitoring points closest to the center of the impact, and the peak and final openings at the monitoring points decreased with the increase of distance of the monitoring points from the impact center. The peak and final crack openings at the monitoring points on the upper crack were less than those at the corresponding points on the lower crack, with the exception of the peak opening at A3, which was larger than the peak opening at a3.

Fig. 18 shows the time-history curves of crack opening at A3 and a3, it is observed from the figure that the variations of the time-history curves of crack opening at A3 and a3 are similar. The peak opening at A3 was 4.40 cm, and the peak opening at a3 was 1.92 cm. The peak openings at A3 and a3 occurred at about 0.45 ms after impact at the peak stage of the impact load. Then, the cracks tended to close as the load of the train's impact diminished, and the final openings were much less than the peak openings.

6. Conclusions

In this paper, the extended finite element method (XFEM) was used to study the dynamic responses of shield tunnel structures with and without a secondary lining upon impact by a derailed train. The crack features of segmental lining and dynamic responses of joint bolts for the shield tunnel structures with and without the secondary lining were compared, and the propagation process and opening evolution of the cracks in the secondary lining were analyzed.

• From the numerical simulation results, it can be found that, when subjected to the train impact load, the cracking damage of segmental lining and the dynamic responses of joint bolts were reduced after using the secondary lining. When subjected to the train impact load, upper and lower cracks appeared in the secondary lining, penetrating through the inner surface to the outer surface. Besides, the crack openings in the secondary lining were larger at the positions close to the impact center, and they decreased as the distance from the center increased.

• According to the simulation results, the secondary lining is capable of enhancing the crashworthiness of the shield tunnel. However, since there is only a small probability that a derailed train will impact a shield tunnel, it is not economically feasible to install secondary linings in all existing shield tunnels to improve their crashworthiness. It is necessary to use an anti-impact secondary lining only in the whole tunnel or part of the tunnel where trains derail easily, e.g., the continuous long-downgrade shield tunnels and the bend parts of the shield tunnel. It is observed from the result that a secondary lining with a thickness of 0.3 m provides a good protective effect. Although this study provided a numerical reference for the design of anti-impact secondary linings, further investigations should be conducted to determine a specific method for determining the design parameters for anti-impact secondary linings.

Acknowledgments

This study was supported by The National Natural Science Foundation of China (No. 51178400; No. 51278425), The Key Project of China Railway Corporation (No. 2014G004-H) and The National Natural Science Foundation of China (No. U1361210).

References

Areias, P.M.A. and Belytschko, T. (2005), "Analysis of three-dimensional crack initiation and propagation using the extended finite element method", *J. Numer. Meth. Eng.*, **63**(5), 760-788.

Baykasoğlu, C., Sünbüloğlu, E., Bozdağ, S.E., Aruk, F., Toprak, T. and Mugan, A. (2011), "Railroad passenger car collision analysis and modifications for improved crashworthiness", *J. Crashworth.*, **16**(3), 319-329.

Belytschko, T. and Black, T. (1999), "Elastic crack growth in finite elements with minimal remeshing", *J. Numer. Meth. Eng.*, **45**(5), 601-620.

Cendón, D.A., Gálvez, J.C., Elices, M. and Planas, J. (2000), "Modelling the fracture of concrete under mixed loading", *J. Fract.*, **103**(3), 293-310.

Fang, X.J., Jin, F. and Wang, J.T. (2007), "Simulation of mixed-mode fracture of concrete using extended finite element method", *Eng. Mech.*, **24**(z1), 46-52.

Feng, K., He, C., Fang Y. and Jiang, Y. (2013), "Study on the mechanical behavior of lining structure for underwater shield tunnel of high-speed railway", *Adv. Struct. Eng.*, **16**(8), 1381-1399.

Gao, G.J. and Tian, H.Q. (2007), "Train's crashworthiness design and collision analysis", *J. Crashworth.*, **12**(1), 21-28.

GB 50010 (2010), *Design of Concrete Structures, Ministry of Housing and Urban-Rural Development of the People's Republic of China*, Beijing, China.

Gupta, N.K. and Venkatesh. (2006), "A study of the influence of diameter and wall thickness of cylindrical tubes on their axial collapse", *Thin. Wall. Struct.*, **44**(3), 290-300.

Hong, S.T., Pan, J., Tyan, T. and Prasad, P. (2008), "Dynamic crush behaviors of aluminum honeycomb specimens under compression dominant inclined loads", *J. Plast.*, **24**(1), 89-117.

Koizumi, A. and He, C. (2000), "Dynamic behavior in longitudinal direction of shield tunnel located at irregular ground with considering effect of secondary lining", *Strain*, **70**(2), 1-9.

Milho, J.F., Ambrósio, J.A.C. and Pereira, M.F.O.S. (2003), "Validated multibody model for train crash analysis", *J. Crashworth.*, **8**(4), 339-352.

Moës, N. and Belytschko, T. (2002), "Extended finite element method for cohesive crack growth", *Eng. Fract. Mech.*, **69**(7), 813-833.

Moës, N., Dolbow, J. and Belytschko, T. (1999), "A finite element method for crack growth without remesh-ing", *J. Numer. Meth. Eng.*, **46**(1), 131-150.

Takamatsu, N., Murakami, H. and Koizumi, A. (1992), "A study on the bending behavior in the longitudinal direction of shield tunnels with secondary linings", *Proceedings of the ITA Congress Towards New Worlds in Tunnelling*, Acapulco, Mexico, May.

Xie, S.C. and Zhou, H. (2014), "Impact characteristics of a composite energy absorbing bearing structure for railway vehicles", *Compos. Part B-Eng.*, **67**, 455-463.

Yan, Q.X., Deng, Z.X., Zhang, Y.Y. and Yang, W.B. (2017), "Failure characteristics of joint bolts in shield tunnels subjected to impact loads from a derailed train", *Shock Vibr.*, **2017**(9), 1-17.

Yan, Q.X., Xu, Y.J., Zhang, W.L., Geng, P. and Yang, W.B. (2018), "Numerical analysis of the cracking and failure behaviors of segmental lining structure of an underwater shield tunnel subjected to a derailed high-speed train impact", *Tunnel. Undergr. Space Technol.*, **72**, 41-54.

Yan, Q.X., Li, B., Geng, P., Chen, C., He, C. and Yang, W.B. (2016), "Dynamic response of a double-lined shield tunnel to train impact loads", *Tunnel. Undergr. Space Technol.*, **53**, 33-45.

Yan, Q.X., Yao C.F., Yang W.B., He, C. and Geng, P. (2015), "An improved numerical model of shield tunnel with double lining and its applications", *Adv. Mater. Sci. Eng.*, **2015**, 1-15.

Zhao, H., Liu, X., Bao, Y. and Yuan, Y. (2017), "Nonlinear simulation of tunnel linings with a simplified numerical modeling", *Struct. Eng. Mech.*, **61**(5), 593-603.

Zia, G., Chen, H., Xu, J. and Belytschko, T. (2005), "The extended finite element method for dynamic fractures", *Shock Vibr.*, **12**(1), 9-23.

CC